



1

2           The review process has now been completed and I am pleased to report that  
3 the paper was accepted for publication on Jul 13, 2021. It is tentatively scheduled for  
4 publication in approximately four months from the date of acceptance.

5

6 Copy edited papers will be posted to the "UMB Online First" section of UMB Online  
7 (<http://www.umbjournal.org/>) and to Elsevier's Science Direct  
8 (<http://www.sciencedirect.com/>) within about two weeks after you approve the proofs.

9

10

11           **Focal bone marrow defects in the jawbone**  
12           **determined by ultrasonography – Validation of new**  
13           **trans alveolar ultrasound technique for measuring**  
14           **jawbone density in 210 patients**

15

16           Johann Lechner<sup>a</sup>

17           Bernd Zimmermann<sup>b</sup>

18           Marlene Schmidt<sup>c</sup>

19

20 <sup>a</sup>Head of Clinic for Integrative Dentistry

21 Gruenwalder Str. 10A

22 81547 Munich,

23 Germany

24

25 <sup>b</sup>Consulting Engineer, QINNO

26 Argelsrieder Feld 11

27 82234 Wessling

28 Germany

29

30 Data Scientist, STEYR Motorenwerke

31 Ramingdorf 21

32 4441 Ramingdorf

33 Austria

34

35 Corresponding author:

36 Dr. Johann Lechner, PhD

37 Gruenwalder Str. 10A

38 81547 Munich

39 Germany

40 Tel: +49-89-6970129

41 Fax: +49-89-6925830

42 E-mail: [drlechner@aol.com](mailto:drlechner@aol.com)

43 **Abstract**

44 Ultrasound imaging of the jawbone is not currently used in dental medicine to  
45 determine bone density. Bone marrow defects in the human jawbone (BMDJ/FDOJ)  
46 are widely discussed in dentistry due to their role in implant failures and as sources of  
47 inflammation in various immune diseases. The use of through-transmission alveolar  
48 ultrasonography (TAU) to locate BMDJ/FDOJ was evaluated using a new TAU  
49 apparatus (TAU-n). The objective was to determine whether the readings displayed by  
50 TAU-n accurately indicate the clinical parameters to detect BMDJ/FDOJ. Three  
51 parameters were compared with TAU-n measurements: 2D-OPG, Hounsfield units  
52 (HU) using digital volume tomography and postoperatively measured levels of  
53 RANTES/CCL5 (R/C) expression in BMDJ/FDOJ samples. Based on the available  
54 clinical data, HU, R/C expression, and TAU-n color codes yielded consistent results  
55 with respect to bone mineral density. Thus, ultrasonography with TAU-n is a reliable  
56 and efficient diagnostic method to screen for BMDJ/FDOJ in dentistry.

57

58 **Keywords:** Bone marrow defects of the jaw, digital volume tomography, fatty-  
59 degenerative osteolysis/osteonecrosis of the jaw, orthopantomogram, RANTES/CCL5,  
60 TAU-n device, transalveolar ultrasonography.

61

62

63

## 64 Introduction

65 In the medical field, ultrasonography is widely used to image various types of  
66 soft tissues. In principle, images of structures in the body are generated by analyzing  
67 the reflection of ultrasound waves. To derive useful information concerning the status  
68 of the jawbone, different ultrasound techniques must be employed as the ultrasound  
69 waves are almost completely reflected at the bone/soft tissue interface. The *in vivo*  
70 measurement of ultrasound velocity in human cortical bone was introduced as a rapid,  
71 reliable, and noninvasive method which could be used to analyze the mechanical  
72 properties of bone (Greenfield et al., 1981). Cortical bone samples showed the highest  
73 values, followed by mixed bone samples and cancellous bone samples, with the latter  
74 showing the lowest values (Kumar et al., 2011). Thus, guided ultrasound waves are  
75 able to detect ischemic bone-marrow diseases, i.e., focal osteoporotic defects or  
76 cavitations in the jawbone (Al-Nawas et al., 2001). Intraoral equipment used in guided  
77 ultrasound must be minimized, however, as the area cannot be examined with  
78 commonly used ultrasound apparatus. Until now, ultrasound examinations have thus  
79 been of limited use in dental medicine, although they have been used to detect “focal”  
80 bone defects of the jawbone, (“focal osteoporotic marrow defects”), as described in  
81 previous scientific research (Kaufman and Einhorn, 1993; Lipani et al., 1982). The  
82 status of cancellous bone in the jaws may be of great clinical importance. Researchers  
83 have provided anatomical evidence that cancellous bone may be significantly  
84 degenerated, a phenomenon described as “ischemic osteonecrosis leading to  
85 cavitational lesions” (Bouquot et al., 1992).

86 The authors of the present study conducted an in-depth investigation of the tissue in  
87 such lesions, which appeared as clumps of fat within intact cortical bone. This tissue  
88 was in an ischemic, fatty-degenerative state. The observed bone marrow defects of  
89 the jaw (BMDJ) were thus defined as “fatty-degenerative osteolysis/osteonecrosis of

90 the jawbone” (FDOJ). The clumps of fat found in the osteolytic jawbone are extremely  
91 biochemically active and produce specific cytokines in high amounts, the most notable  
92 of which is the chemokine RANTES (regulated on activation, normal T-cell expressed  
93 and secreted), or more recently known as CCL5 (chemokine ligand 5; R/C). This  
94 chronic R/C production may influence immunological patterns and exacerbate  
95 systemic immunological diseases (Lechner and Mayer, 2010; Lechner and von Baehr,  
96 2013, 2015; Lechner et al., 2017a, 2017b). The status of cancellous bone in the jaw is  
97 of great importance with respect to dental implants and the success of implantology,  
98 according to previous publications by other authors (Klein et al., 2008; Lee et al.,  
99 2013). One of the most significant concerns associated with the treatment of this  
100 condition, however, is the fact that jawbone with fatty-degenerated bone marrow does  
101 not show signs of abnormal findings on X-ray examination (Lechner, 2014). Being  
102 virtually undetectable on any type of commonly used two-dimensional (2D) X-ray  
103 examination, the occurrence and phenomena of BMDJ/FDOJ remain widely unknown  
104 and are even denied. To overcome this challenge, the use of through-transmission  
105 alveolar ultrasonography (TAU) was evaluated using a new TAU apparatus (TAU-n)  
106 (CaviTAU® QINNO GmbH Argelsrieder Feld 11, 82234 Wessling Germany.  
107 International patent application No: PCT/EP2018/084199. CaviTAU® is approved by  
108 EU medical authorities according to MDD 93/42/EWG

109

110

111

## 112 **Aim and Objectives**

113

114 The aim of the present study was to evaluate BMDJ/FDOJ using TAU-n and to  
115 determine whether TAU-n measurements are practical and capable of promoting

116 quality assurance when assessing BMDJ/FDOJ. Specifically, we aimed to answer the  
117 following questions: Are conventional radiographic techniques suitable to detect  
118 osteolytic bone marrow defects in the jaw (BMDJ/FDOJ), which may display local  
119 silent inflammation? Is a newly available ultrasound device (TAU-n) for the radiation-  
120 free measurement of bone density suitable to visualize the condition of BMDJ/FDOJ  
121 presented above?

122

123

## 124 **Materials and Methods**

125

### 126 *Patient Selection*

127 All 210 patients who were enrolled in this study were seeking to uncover the  
128 etiology of their respective systemic immunological diseases, specifically the  
129 possibility that BMDJ/FDOJ-induced “silent inflammation” of the jawbone may be  
130 involved in the pathogenesis of the disease. The samples and data were taken directly  
131 from daily clinical practice at the Clinic for Integrative Dentistry (Munich, Germany).  
132 Specifically, the data were obtained in the course of the patients’ routine medical care  
133 and were retrospectively evaluated. In cases that necessitated surgical treatment,  
134 samples of BMDJ/FDOJ were postoperatively evaluated to assess the level of R/C  
135 inflammatory markers. Radiographic examinations, namely 2D-OPG and DVT/CBCT,  
136 were assessed to determine bone density and provide the appropriate medical  
137 indication for the surgical treatment of BMDJ/FDOJ in these patients. This indication  
138 was supplemented by bone density measurements using TAU-n. The average age of  
139 the investigation group was 53,02 years; of these patients, there were 129 women and  
140 81 men.

141 The clinical case studies presented here were performed as part of a case-  
142 control study and were deemed to be retrospective in nature. Approval was granted by  
143 the accredited forensic institute, IMD-Berlin, (DIN EN 15189/DIN EN 17025). All  
144 patients provided their written informed consent (as outlined in the PLOS consent  
145 form) to participate in this study. Patients taking bisphosphonates were excluded from  
146 the study. All patients reported that they were not taking vitamin D supplements.

147

## 148 **Preoperative Methods to Determine Bone Marrow Defects in Jawbone** 149 **(BMDJ/FDOJ)**

150

### 151 *Determining BMDJ/FDOJ with conventional 2D-OPGs*

152 Panoramic radiographs are routinely used in clinical dentistry. This imaging  
153 technique is inexpensive and provides a general overview of the entire jaw and  
154 method of initial assessment of the condition of the jaw. The Orangedental PaX-i3D  
155 Duo 3D Multi X-ray unit used in this study displays a "relative bone density"  
156 measurement of the jawbone (rel-JBD) in the 2D-OGP Panoramix version. A red line  
157 shows the measuring range. Figure 1 presents the results of this rel-JBD  
158 measurement: the left image shows the relative density of an all-ceramic crown at 0.9.  
159 The right image shows the relative density of a healthy area of cancellous bone at  
160 0.49.

161

162 Figure 1: Example of measurement of "relative bone density" using OPG.

163 **Notes:** The attenuation coefficients are displayed over the entire test section as a  
164 progression curve. In the present validation, only the mean values (MV) are used.

165 Measurement of relative jawbone density (rel-JBD) values with an Orangedental PaX-  
166 i3D Duo 3D Multi. Legend: Red lines mark the measuring range to display the "relative  
167 density" in the 2D-OPG.

168

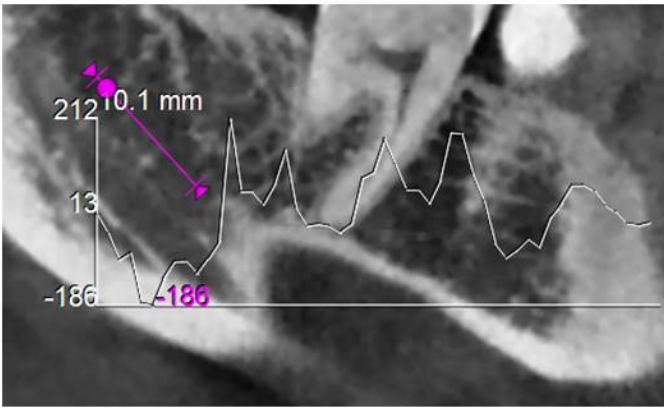
169

#### 170 *Determining BMDJ/FDOJ with 3D-CBCT/DVT*

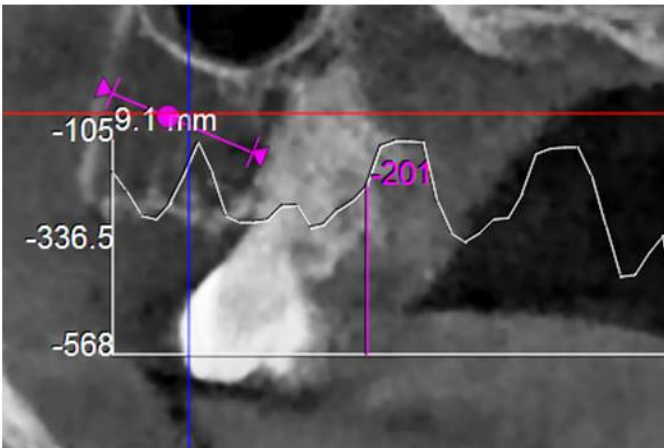
171 Modern X-ray methods, like digital volume tomography (DVT), allow the  
172 clinician to perform a 3D assessment of the jawbone using Hounsfield units (HU),  
173 which are generally scientifically recognized as a bone density assessment tool. HU  
174 are used to describe the attenuation of X-ray radiation in tissues and this information  
175 is displayed in grayscale images. The HU scale ranges from -1,000 (attenuation  
176 coefficient of air) to -120 (fat), +300 to +400 (healthy cancellous bone), and +1,800 to  
177 +2,200 (cortical bone). Water is defined as 0 HU. Recently, methods to determine HU  
178 attenuation coefficients have become available (Norton and Gamble, 2001), as actual  
179 HU values can be derived using DVT (Misch, 1999; Swennen and Schutyser, 2006).  
180 Further investigations classified the density of cancellous bone in the jawbone into five  
181 categories, where the poorest jawbone density was below 150 HU (class 5). In this  
182 study, we used specific DVT equipment (Orangedental PaX-i3D Duo 3D Multi X-ray)  
183 with the appropriate software to evaluate the density of the jawbone in HU. In  
184 accordance with DIN 6868-57, the viewing monitors were set with a contrast of >40:1  
185 and a brightness of at least 120 cd/m<sup>2</sup>. The Orangedental PaX-i3D Duo 3D Multi X-ray  
186 machine used in this validation study showed the mean value of a randomly selected  
187 measurement path, with the maximum and minimum values presented as a  
188 progression curve (Figure 2).

189





Area 48-49  
 HU -186 bis 212  
 MV=13



Area 18-19  
 HU -568 bis -105  
 MV= -336.5

190  
 191 Figure 2. Example of a DVT HU measurement and evaluation of BMDJ/FDOJ: The HU  
 192 attenuation coefficients are shown as a curve over the measured section. In the  
 193 present validation study, only the mean values (MV) are used.

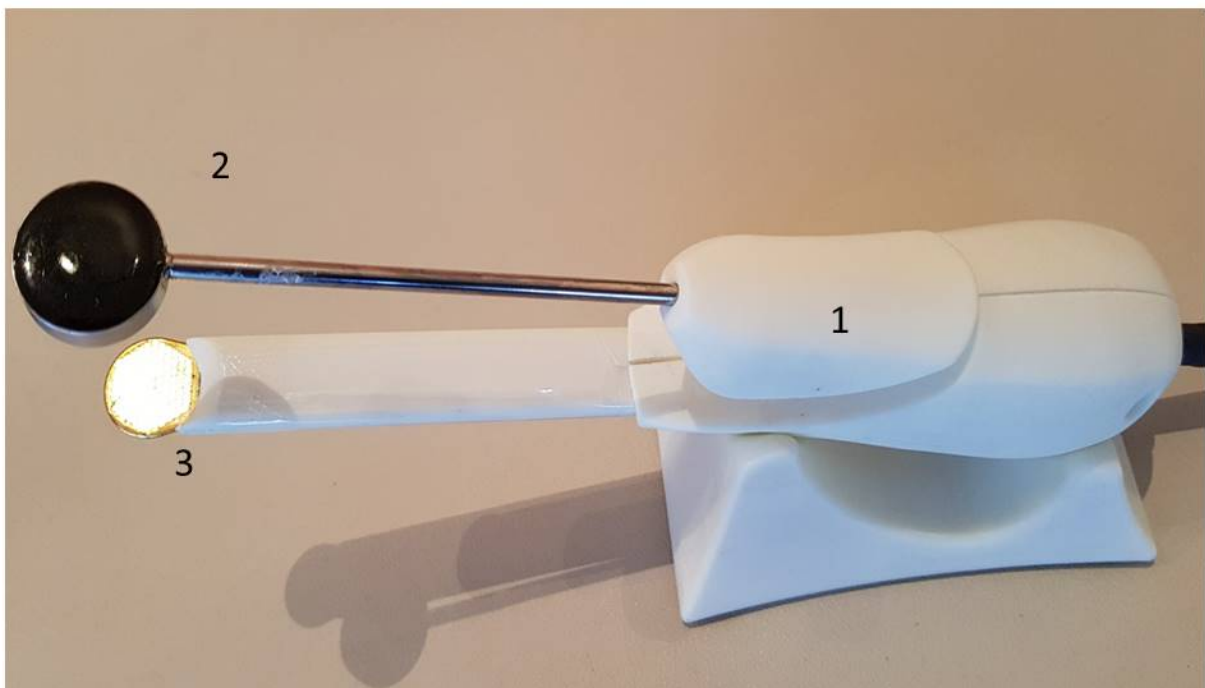
194

195

196 *Determining BMDJ/FDOJ with TAU-n using ultrasound waves*

197 Attenuation in the amplitude of the ultrasound wave is indicative of pathological  
 198 changes in the jawbone and depends on the properties of the medium through which  
 199 the wave is propagated (Mahmoud et al., 2008). Corresponding values are based on  
 200 the published data from Wells (1999) and Njeh et al. (1999). TAU-n generates an  
 201 ultrasound wave and passes that wave through the jawbone. This wave is produced  
 202 by an extraoral transmitter and then detected and measured by a receiving unit that  
 203 is positioned intraorally. Both parts (i.e., the sender and receiving unit) are fixed in a

204 parallel position using a single handpiece. The size of the TAU-n receiving unit is  
205 configured such that it may be easily placed inside the mouth of a patient. TAU-n uses  
206 91 piezoelectric elements that are arranged hexagonally. The jawbone must be  
207 positioned between the two parts of the measuring unit. With respect to the parts of  
208 the measuring unit to be placed inside a patient's mouth, the acoustical coupling  
209 between those parts and the alveolar ridge is performed with the aid of a semi-solid  
210 gel (QINNO GmbH Argelsrieder Feld 11, 82234 Wessling Germany). The contact  
211 between the jawbone and both the extraoral ultrasound transmitter and intraoral  
212 ultrasound receiver (Figure 3) is optimized and individualized using a special  
213 ultrasound gel cushion that was developed for this purpose. The results are shown on  
214 a color monitor that displays different colors depending on the degree of attenuation. A  
215 semi-solid, single-use gel pad is used around the receiver for hygienic reasons (Figure  
216 4).

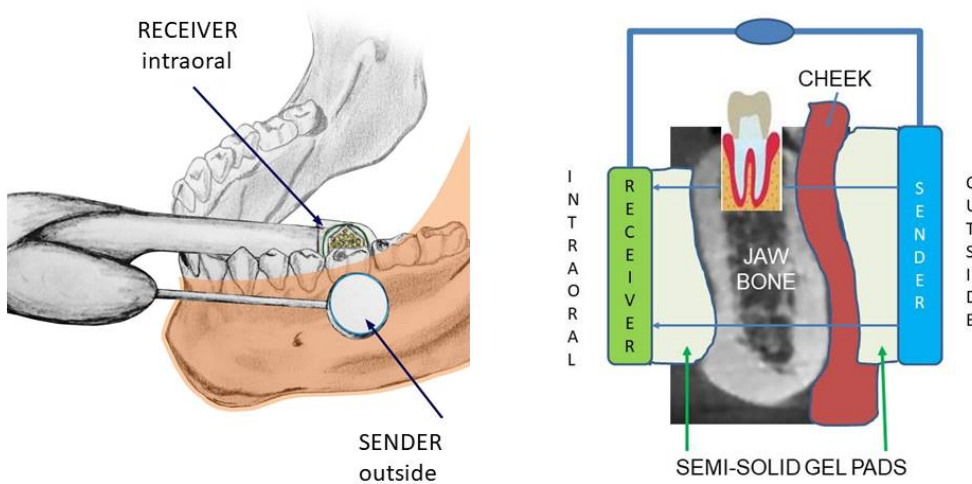


217

218 Figure 3. Legend: (1) Handpiece with an ultrasound sender and receiver unit  
219 connected to a computer and screen. (2) Ultrasound transmitter. (3) Ultrasound  
220 receiver with 91 piezoelectric elements. Coplanar and fixed arrangement of the sender  
221 and receiver.

222

223



224

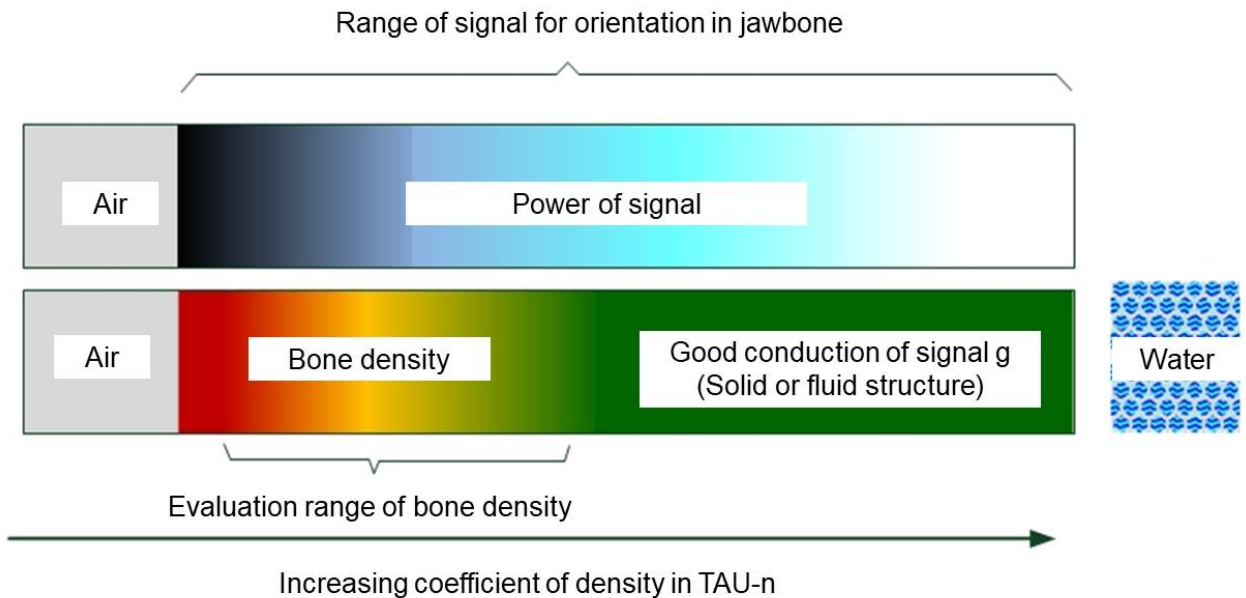
225 Figure 4. Legend: Left panel: Positioning of the sender (outside) and receiver  
226 (intraoral) in the lower jaw; red area marks the cheek. Right panel: The sender (in blue  
227 on the right) and receiver (in green on the left) are in a fixed coplanar position (a blue  
228 bar connects the sender and receiver); semi-solid gel pads between the sender and  
229 the cheek on the outside of the mouth and between the receiver and the alveolar ridge  
230 in the intraoral position; trans-alveolar ultrasonic impulse from the sender to receiver  
231 (blue arrows).

232

233 *Color scale associated with TAU-n attenuation coefficients*

234 Figure 5 presents the color scheme associated with the TAU-n attenuation  
 235 coefficients. This scheme corresponds to an ultrasound signal strength scale (top bar)  
 236 and a color scale indicating the different degrees of bone density (lower bar). This  
 237 color scale shows that the colors used to indicate different densities each represent a  
 238 small part of the entire signal range. Logarithmic averaging broadens the range of  
 239 bone density measurements and increases the size of the area in green.

240  
 241  
 242 The representations of the measurements provided by the color coding scheme  
 243 are concerned with two functions. With the red/green color scale, the medically  
 244 relevant area of conspicuousness bone is shown. The second color coded scale  
 245 shows structural differences which serves as an orientation aid for the user for the  
 246 placement of the measuring receiver. In this way, the orientation and position of the  
 247 receiver may be monitored (via live display) while the measurement position is slowly  
 248 adjusted before the relevant area is captured and stored.



249

250 Figure 5. The color scale is used to indicate different degrees of density by TAU-n;  
251 gray corresponds to air (i.e., the far left of the scale), and the blue area corresponds to  
252 water (i.e., the far right of the scale). The signal strength received by the sensor (top  
253 bar) is displayed in blue and increases from dark to light with increasing density  
254 coefficients. Bone density (lower bar) is indicated by a colour scale ranging from red  
255 to green, representing the high attenuation of diminished bone density (red) and  
256 reduced attenuation with increasing density (green).

257

258

### 259 *The TAU-n display*

260 The TAU-n display is able to capture the following physical structures in the  
261 dentoalveolar region, with the corresponding color variations of 91 color columns per  
262 cm<sup>2</sup>: (A) solid bone in the marginal cortical area (green or white/light blue); (B) healthy  
263 medullary cancellous bone (green or white/light blue); (C) chronic inflammatory  
264 medullary cancellous bone with fatty-degenerative components (red or black/dark  
265 blue); (D) fatty nerve structures (yellow/ light blue); and (E) extremely dense and  
266 complex structures such as teeth, implants, and crowns (green or white/light blue)  
267 (Figure 6).



268  
 269 Figure 6. Example of the color coding scheme associated with attenuation used by  
 270 TAU-n in area 38.

271 **Notes:** In the upper panel, the measurement of jaw areas 37 to 38/39 (i.e., the  
 272 retromolar area) is presented. TAU-n displays different degrees of mineralization, as  
 273 highlighted by the various color patterns of 91 individual sensor fields that correspond  
 274 to each jawbone area. Green: indicates hard and dense structures that correspond to  
 275 a higher degree of mineralization in spongy jawbone or cortical bone; green also  
 276 denotes teeth, dental crowns, or implants. Yellow: indicates diminished bone density,  
 277 and also corresponds to the nerve canal in the lower jaw. Red: indicates severely  
 278 diminished bone density with a low degree of mineralization, corresponding to  
 279 BMDJ/FDOJ areas.

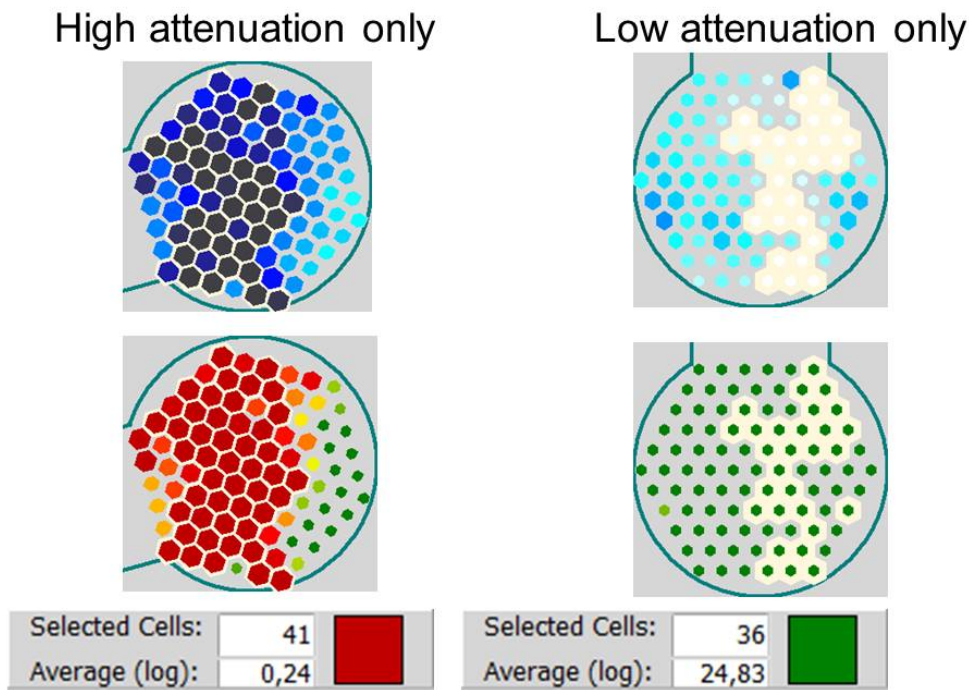
280

281

282

283 *Numerical representation of TAU-n attenuation coefficients*

284 The TAU-n software numerically represents the attenuation coefficients of the  
 285 TAU-n measurement range. By a mouse click on one of the 91 sensor fields of a given  
 286 measurement, the software marks the field and displays the measured value in a  
 287 logarithmic evaluation. The sensor fields that show the highest attenuation values  
 288 defined by TAU-n are marked in either red or black, and this indicates the bone  
 289 density of an area of BMDJ/FDOJ. TAU-n computes the logarithmic average of the  
 290 sum of the sensor elements with the lowest density unit as "Average(log)", displayed  
 291 in red (Figure 7, left panel). In the same way, the logarithmic average of the sensor  
 292 elements with the highest density – equivalent to reduced attenuation by solid  
 293 structures – is displayed in green (Figure 7, right panel). In the following sections and  
 294 Table 1, the term "TAU-n log" is used to represent the numbers of "Average(log)"  
 295 displayed by TAU-n.  
 296



297  
 298 Figure 7. Sensor elements. **Notes:** Numerical representation of the TAU-n attenuation  
 299 coefficients for diminished bone density (left panel) and for dense material (right

300 panel). Selected sensor cells (left panel: high attenuation; right panel: low attenuation)  
301 are indicated by a white border. The evaluation is presented in the window beneath for  
302 a number of selected sensor cells; the result is displayed as a logarithmic mean, which  
303 is associated with a corresponding color (i.e., left panel: red = / corresponds to high  
304 attenuation; right panel: green = / corresponds to low attenuation).

305

306

307

308

### 309 *Problems of acoustic coupling in TAU-n*

310 The practical application of the transducer and receiver with fixed geometrical  
311 positions to obtain intraoral ultrasonic measurements (i.e., within the mouth of a  
312 patient) with sufficient acoustical conductivity proved to be difficult. The ultrasonic gel,  
313 which was placed inside the patient's mouth, was shown to be the main obstacle when  
314 attempting to obtain signals from TAU-n in an easy and reproducible manner. The  
315 primary difficulty is ensuring that the ultrasonic gel is completely free from air bubbles  
316 given the high viscosity of the gel. Air bubbles interfere with obtaining reliable and  
317 repeatable measurements. In addition, the study team found that the anatomical  
318 contour of the jawbone at the site of measurement and the plane surface of the  
319 intraoral receiver did not adequately conform to one another. The distance between  
320 the surface of the receiver and that of the alveolar ridge was shown to vary widely.

321 As a solution, a semi-solid gel pad was placed between the receiver and the  
322 alveolar ridge of the patient. The sound velocity in the gel used should fall within the  
323 same range as that of soft tissue (i.e., 1,460–1615 m/s) and the gel should have a  
324 sound attenuation ranging from 0.3–1.5 dB/cm (1 MHz), so as not to impede the  
325 acoustical measurements in the jawbone. The haul-off speed for spontaneous



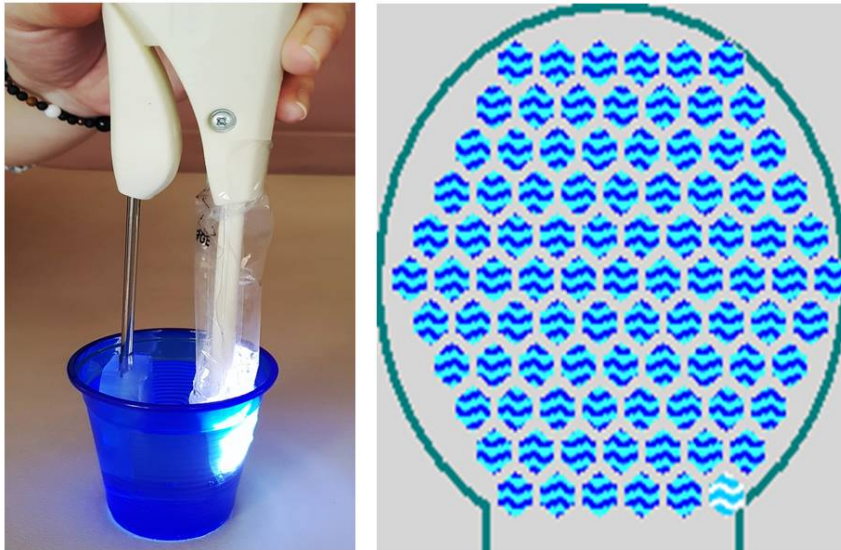
326 resilience should not exceed 80 mm/s. The semi-solid property of the gel prevents it  
327 from evaporating/disappearing before or during the measurement. To perform the  
328 measurements, inside the gel pad is a small pocket into which the receiver can be  
329 inserted. Following the elimination of any air bubbles between the receiver and the  
330 semi-solid gel, the measuring unit is ready for use.

331

### 332 *Calibration of TAU-n*

333         The arrangement of the measuring unit in a defined geometry allows for the  
334 easy calibration of TAU-n. This functional test is performed with flexible gel pads  
335 covering both the transmitter and receiver. Figure 8 illustrates the procedure, i.e., the  
336 full immersion of both parts into a vessel filled with water. The complete acoustic  
337 coupling is visible when all sensor elements show the watermark in the left image of  
338 the sensor on the computer display. This calibration in a water bath at constant  
339 conditions allows for the compensation of possible deviation of the elements as a  
340 starting point for the measurement. The calibration test ensures that no air pockets  
341 interfere in the arrangement with cushions, gel, and sleeves and that no failure of  
342 elements or components leads to misinterpretation.

343



344  
345 Figure 8. Water test for calibration: Left panel: Transmitter and receiver must be  
346 completely submerged in water. Right panel: All sensor elements show  
347 watermarks with the exception of the lower right sensor element.

348

349

### 350 **Postoperative Method to Determine BMDJ/FDOJ**

351

#### 352 *Determining BMDJ/FDOJ with RANTES/CCL5 (R/C) expression*

353 BMDJ/FDOJ cavitations contain degenerated adipocytes that exhibit a  
354 particular expression profile of the chemokine R/C (Lechner and Mayer, 2010;  
355 Lechner and von Baehr, 2013, 2015; Lechner et al., 2017a, 2017b). Hence,  
356 BMDJ/FDOJ samples were also analyzed for the expression of the inflammatory  
357 immune mediator R/C. Laboratory procedures used to define R/C expression levels in  
358 the healthy jawbone and in BMDJ/FDOJ have been previously published; healthy  
359 jawbone showed R/C expression levels of 149 pg/mL, while a significant number of  
360 BMDJ/FDOJ samples (n=301) among patients with chronic disease (average age:  
361 54.05 years; age range: 23–75 years; gender ratio: 89 females to 225 males) showed

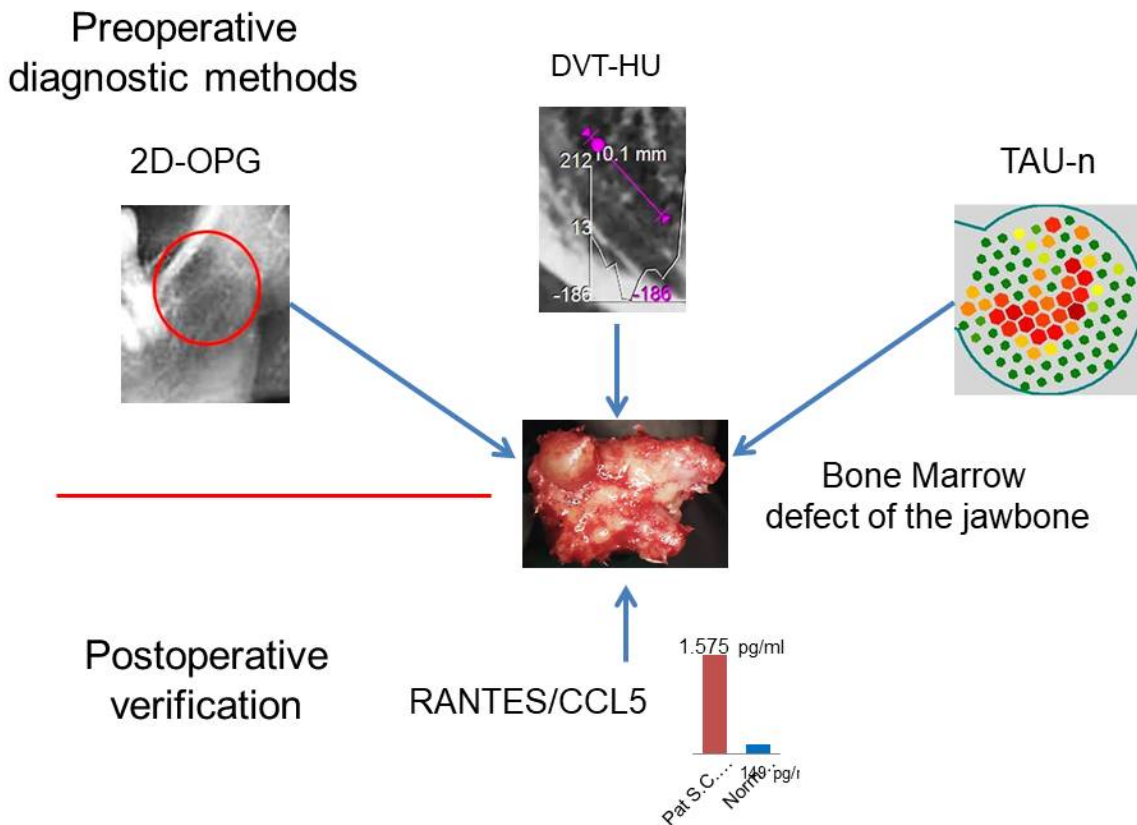
362 a 20-fold increase in R/C expression of 2,940 pg/mL (Lechner and Mayer, 2010;  
363 Lechner and von Baehr, 2013, 2015; Lechner et al., 2017a, 2017b). BMDJ/FDOJ are  
364 the only bone resorption processes that show R/C overexpression (Lechner et al.,  
365 2018). BMDJ/FDOJ also display a reduction in tumor necrosis factor (TNF)- $\alpha$  and  
366 interleukin (IL)-6 expression, while all other bone resorption-related diseases are  
367 characterized by TNF- $\alpha$  and IL-6 overexpression. In summary, the recent literature  
368 has shown that BMDJ/FDOJ are not only characterized by reduced mineralization and  
369 diminished bone density, but also play an important role in osteoimmunological  
370 processes. Thus, R/C overexpression alone is involved in the characteristic and bone-  
371 degrading aspect of BMDJ/FDOJ (Lechner et al., 2018).

372 Based on findings of publications and in the literature (Lechner and Mayer, 2010;  
373 Lechner and von Baehr, 2013, 2015; Lechner et al., 2017a, 2017b), it is known that an  
374 R/C expression level higher than 149 pg/mL indicates the presence of osteonecrosis  
375 or osteolysis which has resulted in diminished jawbone density. A control group of 19  
376 patients volunteered to provide samples of healthy jawbone, which were removed  
377 using drill cores during dental implantation surgery. The inclusion criteria for this group  
378 were as follows: the absence of distinctive radiological features in 2D-OPG and 3D-  
379 DVT; inconspicuous TAU-n measurements of bone density in the implantation area.  
380 The use of bisphosphonate medication was the central exclusion criterion. The  
381 demographic data of the 19 cases in the BMDJ/FDOJ control group were: average  
382 age, 51.4 years; age range, 33–72 years; gender (female/male): 10/9.

383  
384 *Collection of preoperative rel-JBD, HU and TAU-n values and postoperatively*  
385 *measured levels of RANTES/CCL5 expression in a group of 210 patients with*  
386 *BMDJ/FDOJ.*

387 In this study, a patient cohort of 210 subjects that exhibited clinical evidence of  
 388 BMDJ/FDOJ (i.e., an HU value, a local R/C expression profile, and TAU-n  
 389 measurements) was identified to investigate our research objective in a clinical setting.  
 390 The schematic representation in Figure 9 illustrates the four validation parameters  
 391 discussed and employed in this study. Each of the subjects in this group was  
 392 assessed with TAU-n. To be included in this group, each patient was required to have  
 393 the following with respect to the area of BMDJ/FDOJ investigated: positive  
 394 preoperative TAU-n measurements, low bone density (in HU values), and a  
 395 postoperative evaluation of R/C expression. We compared the preoperative TAU-n  
 396 and HU values of the research group with the postoperatively obtained laboratory  
 397 results of R/C expression of the corresponding jawbone areas of BMDJ/FDOJ.

398  
 399



400

401 Figure 9. The possible methods used to localize BMDJ/FDOJ. **Notes:** Preoperative  
402 2D-OPG is insufficient, while DVT with the possibility of HU measurement may provide  
403 a clear indication of BMDJ/FDOJ. The use of TAU-n as a novel, radiation-free  
404 measurement option is evaluated in this report. Postoperative multiplex analysis  
405 shows extreme R/C overexpression, providing evidence of inflammation.

406

407

#### 408 *Statistical analysis*

409 The statistical analysis was conducted using the statistical software R version  
410 3.5.1. The similarity between the HU and TAU-n methods was verified by means of  
411 Spearman's correlation coefficient.

412

413

#### 414 **Results**

415 *Comparison of preoperative TAU-n and HU values with postoperative evaluation of*  
416 *RANTES/CCL5 expression in a group of 210 patients with BMDJ/FDOJ*

417 After evaluating the detection of BMDJ/FDOJ using TAU-n, we established  
418 clinical evidence of the TAU-n attenuation coefficients by comparing and verifying  
419 preoperative HU and TAU-n values with the postoperatively determined R/C  
420 expression levels of corresponding BMDJ/FDOJ areas. The results are shown in  
421 Table 1. In Figure 9, we present three preoperative methods and one postoperative  
422 method used to assess BMDJ/FDOJ. For this group of 210 patients, we carried out  
423 each of these four methods and compared the results, i.e., (B) the preoperative HU  
424 attenuation coefficients; (C) the corresponding TAU-n attenuation coefficients of  
425 BMDJ/FDOJ according to "Average(log)" in the TAU-n software (TAU-n Log in Table

426 1; see Figure 7); and (D) the R/C expression levels in the fatty degenerated samples

427 obtained during BMDJ/FDOJ surgery (Table 1).

Patient#	OPG	HU	AvLog CaviTAU	RANTES pg/ml
1	0,6	-29,0	1,35	8.212,50
2	0,4	-96,0	1,41	2.762,50
3	0,7	-533,0	0,67	5.700,00
4	0,75	-326,0	4,49	3.250,00
5	0,3	-316,0	0,3	3.925,00
6	0,5	-591,0	0,33	3.762,50
7	0,6	-295,0	0,36	2.162,50
8	0,4	-93,0	0,44	2.187,50
9	0,4	-250,0	0,84	2.850,00
10	0,65	-745,0	1,58	722,50
11	0,55	-263,0	0,84	1.825,00
12	0,5	-311,0	0,46	1.787,50
13	0,45	89,0	0,67	1.725,00
14	0,4	-300,0	1,37	5.387,50
15	0,45	-340,0	0,87	992,50
16	0,5	-306,5	1,04	2.512,50
17	0,3	-228,5	0,82	2.362,50
18	0,65	11,5	0,9	3.862,50
19	0,6	-58,5	0,64	457,50
20	0,5	-659,0	0,85	873,75
21	0,35	-447,0	0,31	706,25
22	0,4	-431,0	0,83	2.825,00
23	0,4	-31,5	0,64	1.165,00
24	0,55	-450,0	1,12	405,00
25	0,45	-565,0	0,69	146,25
26	0,4	-68,0	0,72	766,25
27	0,55	-647,0	2,58	5.525,00
28	0,5	54,5	1,52	7.275,00
29	0,6	-549,0	0,82	2.112,50
30	0,4	-130,0	0,76	2.575,00
31	0,65	120,5	0,94	5.562,50
32	0,7	-345,0	0,95	1.612,50
33	0,6	-77,5	0,58	205,00
34	0,65	72,5	1,85	2.962,50
35	0,55	-173,0	1,07	1.875,00
36	0,5	-249,0	0,66	267,50
37	0,4	-413,0	0,38	1.750,00
38	0,7	-291,0	0,52	1.887,50
39	0,6	-238,5	1,32	2.000,00
40	0,6	-537,0	1,22	1.337,50
41	0,65	-676,0	0,79	702,50
42	0,4	-62,0	0,54	846,25
43	0,4	-179,5	2,58	408,75
44	0,6	-243,0	1,26	810,00
45	0,4	-560,0	1,5	518,75
46	0,6	-494,0	0,84	486,25
47	0,55	-387,0	0,75	2.875,00
48	0,6	-379,0	1,14	2.737,50
49	0,4	-228,0	0,32	2.425,00
50	0,5	-440,0	0,68	1.078,75
51	0,6	-308,0	0,54	1.800,00
52	0,6	-322,0	1,21	19.125,00

53	0,5	-589,0	2,29	645,00
54	0,55	-518,0	1,21	1.575,00
55	0,45	-294,0	0,51	2.187,50
56	0,55	-671,0	0,89	767,50
57	0,55	-244,0	1,89	580,00
58	0,3	-573,0	1,77	8.062,50
59	0,65	-454,0	0,93	910,00
60	0,4	99,0	1,57	5.025,00
61	0,2	-182,5	1,78	4.562,50
62	0,6	-335,0	1,03	3.725,00
63	0,4	-288,0	0,79	3.587,50
64	0,5	-132,0	1,75	840,00
65	0,6	-202,0	1,03	2.300,00
66	0,3	-418,0	0,81	5.362,50
67	0,45	-290,0	1,38	1.637,50
68	0,6	-41,0	0,96	636,25
69	0,4	-184,0	1,67	2.200,00
70	0,5	-227,0	1,11	863,75
71	0,6	-198,0	1,38	1.587,50
72	0,45	-261,0	1,65	3.987,50
73	0,55	-543,0	1,01	3.937,50
74	0,6	-363,0	1,19	1.275,00
75	0,45	-268,0	0,32	10.150,00
76	0,55	-110,0	1,69	573,75
77	0,75	-248,0	1,61	1.337,50
78	0,65	-142,0	1,28	611,25
79	0,35	-264,0	2,51	893,75
80	0,45	-301,0	0,86	2.100,00
81	0,5	-654,0	1,05	866,25
82	0,75	-168,0	1,53	1.775,00
83	0,4	146,0	0,79	1.400,00
84	0,4	123,0	1,37	1.800,00
85	0,4	-222,0	0,77	1.925,00
86	0,6	-36,0	1,23	303,75
87	0,4	-5,0	1,15	1.215,00
88	0,25	-213,0	1,52	412,50
89	0,5	88,0	1,24	495,00
90	0,25	-347,0	1,19	1.600,00
91	0,45	45,0	1	1.725,00
92	0,4	-38,0	0,47	527,50
93	0,5	160,0	1,28	3.612,50
94	0,5	-313,0	0,82	1.337,50
95	0,55	119,0	1,38	1.192,50
96	0,4	-196,0	0,8	1.246,25
97	0,55	-17,0	0,96	638,75
98	0,3	-457,0	0,47	6.512,50
99	0,3	-373,0	0,7	456,25
100	0,5	-209,0	1,25	3.275,00
101	0,4	-438,0	0,81	2.262,50
102	0,5	-38,0	0,88	447,50
103	0,45	-404,0	0,47	746,25
104	0,35	-170,0	1,64	1.400,00

428

105	0,4	126,0	1,07	436,25
106	0,55	103,0	1,05	588,75
107	0,4	96,0	0,84	1.312,50
108	0,7	162,0	0,97	1.500,00
109	0,6	-66,0	1,12	223,75
110	0,45	-105,0	1,21	373,75
111	0,5	-20,0	0,98	277,50
112	0,5	-208,0	1,58	705,00
113	0,6	-264,0	1,8	1.912,50
114	0,6	-83,0	0,81	3.962,50
115	0,6	-38,0	0,67	432,50
116	0,4	-348,0	1,33	1.675,00
117	0,4	150,0	1,17	311,25
118	0,4	-166,0	1,35	1.023,75
119	0,55	144,0	1,37	996,25
120	0,45	-94,0	1,71	498,75
121	0,5	41,0	2,67	3.187,50
122	0,5	-157,0	1,4	417,50
123	0,45	-291,0	0,61	1.325,00
124	0,6	77,0	1,17	917,50
125	0,35	-96,0	1,89	1.687,50
126	0,4	4,0	0,98	228,75
127	0,25	-183,0	1,58	355,00
128	0,45	-43,0	1,18	407,50
129	0,4	-147,0	0,36	541,25
130	0,4	-145,0	0,73	408,75
131	0,4	-245,0	0,73	572,50
132	0,65	150,0	1,24	1.600,00
133	0,4	-87,0	1,59	586,25
134	0,2	-138,0	1,38	1.287,50
135	0,5	-27,0	1,09	945,00
136	0,35	-257,0	1,22	647,50
137	0,35	-120,0	0,31	267,50
138	0,35	-116,0	0,95	233,75
139	0,55	-30,0	1,38	572,50
140	0,4	150,0	1,57	673,75
141	0,6	-155,0	1,12	2.862,50
142	0,55	157,0	1,11	691,25
143	0,5	-127,0	0,67	1.650,00
144	0,3	-110,0	0,93	565,00
145	0,55	84,0	0,84	1.137,50
146	0,45	-414,0	0,87	8.087,50
147	0,45	-122,0	1,53	1.217,50
148	0,4	-145,0	1,5	4.075,00
149	0,6	170,0	0,67	562,50
150	0,5	97,0	0,97	1.337,50
151	0,45	197,0	0,5	1.875,00
152	0,6	-117,0	1,6	950,00
153	0,4	-363,0	1,95	1.111,25
154	0,35	16,0	1,26	4.437,50
155	0,55	-123,0	0,76	2.750,00
156	0,4	23,0	1,58	370,00
157	0,35	52,0	1,48	370,00

158	0,35	320,0	0,58	518,75
159	0,4	-108,0	0,36	1.475,00
160	0,6	-23,0	1,04	5.175,00
161	0,4	-566,0	1,26	873,75
162	0,5	-55,0	1,28	2.637,50
163	0,45	-305,0	0,85	486,25
164	0,5	93,0	1,9	460,00
165	0,55	42,0	0,75	457,50
166	0,5	59,0	1,46	1.312,50
167	0,5	-175,0	0,96	5.462,50
168	0,4	-450,0	1,07	11.437,50
169	0,5	107,0	1,66	1.163,75
170	0,45	-8,0	1,86	650,00
171	0,6	192,0	1,56	1.300,00
172	0,35	43,0	0,62	573,75
173	0,45	-120,0	0,73	190,00
174	0,6	-96,0	1,35	966,25
175	0,55	-58,0	1,09	3.137,50
176	0,25	-69,0	0,77	3.225,00
177	0,5	-420,0	0,94	978,75
178	0,4	-225,0	0,84	2.675,00
179	0,35	123,0	0,89	2.287,50
180	0,6	-115,0	0,7	1.825,00
181	0,3	-63,0	1,31	1.250,00
182	0,4	-175,0	1,57	1.108,75
183	0,6	97,0	1,79	1.425,00
184	0,5	2,0	1,56	1.750,00
185	0,55	179,0	1,5	647,50
186	0,45	40,0	1,89	968,75
187	0,4	65,0	0,67	733,75
188	0,7	200,0	1,41	555,00
189	0,5	-44,0	1,23	1.950,00
190	0,35	-58,0	1,44	631,25
191	0,4	-116,0	1,34	2.362,50
192	0,35	-293,0	1,28	338,75
193	0,35	153,0	0,71	985,00
194	0,5	-316,0	1,32	1.600,00
195	0,2	-231,0	0,35	4.574,00
196	0,5	-162,0	1,09	3.400,00
197	0,4	-94,0	0,73	1.675,00
198	0,6	167,0	1,89	370,00
199	0,45	-62,0	1,25	324,00
200	0,55	-327,0	1,01	1.132,00
201	0,6	-210,0	1,02	863,00
202	0,35	-197,0	1,42	2.350,00
203	0,5	-550,0	1,88	1.850,00
204	0,6	-290,0	0,32	863,00
205	0,5	-68,0	1,22	2.887,00
206	0,3	-192,0	1,48	7.912,00
207	0,5	63,0	1,56	1.625,00
208	0,5	37,0	1,1	2.237,00
209	0,45	-57,0	1,28	950,00
210	0,6	-154,0	0,73	661,00
	<b>0,48</b>	<b>-165,7</b>	<b>1,2</b>	<b>1950,38</b>

429

430

431

432

433 Table 1: This table presents the four values measured to assess BMDJ/FDOJ for a  
434 group of 210 patients. The four relevant values are listed individually for each patient.  
435 The mean value obtained preoperatively for 2D-OPG was a relative bone density of  
436 0.48; for 3D-DVT HU the value was -165.7 (norm = >300) and for CaviTAU®  
437 AverageLog the value was 1.2 (normal bone density >2.0). For R/C expression, the  
438 mean was 1,950.38 pg/ml (norm = 149.9 pg/ml). **Notes:** Comparison of preoperative  
439 HU attenuation coefficients and corresponding TAU-n attenuation coefficients (TAU-n  
440 Log; columns in grey), and postoperatively measured levels of R/C expression  
441 (RANTES pg/mL) from the samples obtained during surgical treatment for  
442 BMDJ/FDOJ (columns in blue). MV refers to the medium values obtained in the  
443 course of our research, and the final row compares the corresponding values of  
444 healthy jawbone found in the literature (HU; Guglielmi and de Terlizzi, 2009; Komar  
445 et al., 2019; Mah et al., 2010) and RANTES levels (pg/mL; Klein et al., 2008; Lechner  
446 and Mayer, 2010; Lechner and von Baehr, 2013, 2015; Lechner et al., 2017a,  
447 2017b).

448

#### 449 *Comparison of rel-JBD, HU, and TAU-n values of healthy jawbone*

450 To ensure that TAU-n generates significantly higher attenuation values in  
451 jawbone where BMDJ/FDOJ is not present, we measured rel-JBD, HU, and TAU-n  
452 values in healthy jawbone. To obtain valid negative results, we focused on bone  
453 marrow areas beneath healthy molar teeth. The process of determining rel-JBD and  
454 HU was shown above in Figure 1. The results obtained for healthy jawbone in 10  
455 patients are presented in Table 2. R/C values were unable to be measured as  
456 surgical intervention in areas of healthy jawbone was not possible for ethical  
457 reasons.

458



459 Table 2

460

Patient	area	OPG	HU	TAU	
pat#1		37	0,55	272	7,02
pat#2		37	0,5	599	8,49
pat#3		47	0,55	97	4,46
pat#4		37	0,45	193	7,14
pat#5		36	0,55	678	6,89
pat#6		37	0,45	271	11,51
pat#7		36	0,35	744	6,71
pat#8		46	0,6	306	10,51
pat#9		47	0,4	329	6,16
pat#10		37	0,4	315	9,79
MV			0,48	380,4	7,868

461

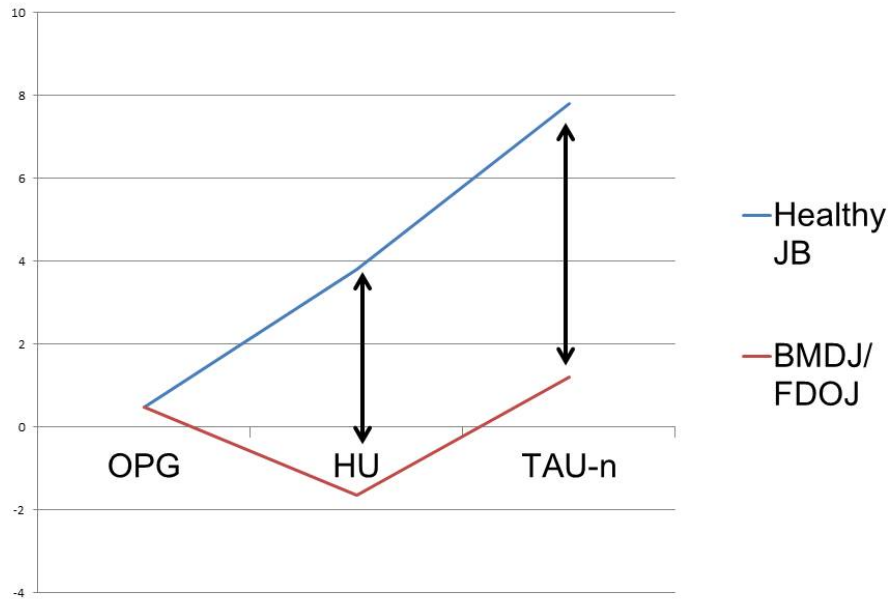
462 Table 2. Measurement of rel-JBD, HU, and TAU-n values in healthy jawbone.

463

464 *Comparison of rel-JBD, HU, and TAU-n values of healthy jawbone and BMDJ/FDOJ*  
465 *areas*

466 The bone density measured in healthy jawbone and BMDJ/FDOJ areas are  
467 compared as mean values. There is clear agreement in the rel-JBD values obtained  
468 with 2D-OPG, (4,8 BMDJ/FDOJ : 4,8 healthy), while the HU values (-165  
469 BMDJ/FDOJ : 380 healthy) and particularly TAU-n values (1,2 BMDJ/FDOJ : 7,8  
470 healthy) differ significantly (Figure 10).

471



472

473 Figure 10. This graph shows the comparison of relative bone density values  
 474 determined with 2D-OPG, attenuation coefficients in HU (1:100) and TAU-n values in  
 475 healthy and BMDJ/FDOJ collectives.

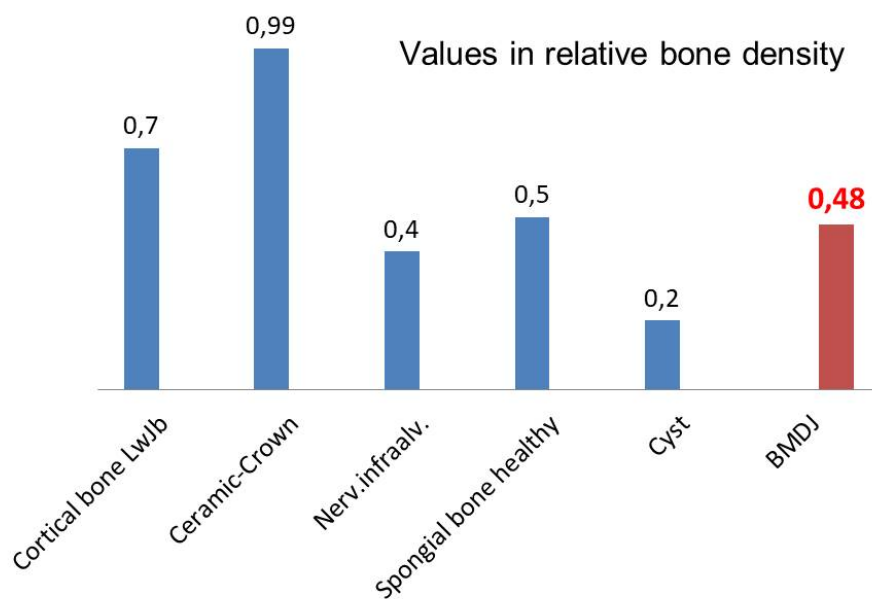
476

477

478 **Discussion**

479 *On "bone marrow defects" and 2D-OPG*

480 In order to compare the results documented in Table 1 in terms of their clinical  
 481 significance, we calculated 10 mean values of jawbone density measurements  
 482 obtained with 2D-OPG from three different dental colleagues with available  
 483 radiographs. The five control parameters comprised the following measurements:  
 484 cortical bone on the mandibular branch, all-ceramic crown, the canal of infra alveolar  
 485 nerve, cancellous bone normal and cyst lumen. Figure 11 shows these values in  
 486 blue. Bone density values in areas of BMDJ/FDOJ collected from the cohort of 210  
 487 patients are presented in red.



488

489 Figure 11: Comparison of various density values with BMDJ/FDOJ values obtained  
 490 using 2D-OPG. This shows that normal bone density measured in healthy spongiel  
 491 cancellous bone structure with a value of 0.5 is only slightly "denser" than the mean  
 492 value of the 210 BMDJ/FDOJ areas we examined with a medium value of 0.48. This  
 493 explains, in part, the/is one reason why there is widespread doubt among dentists in  
 494 the discussion about/concerning the actual existence of BMDJ/FDOJ. In summary, a  
 495 critical detection of medullary bone density in BMDJ/FDOJ areas is not possible with  
 496 2D-OPG (Lechner J. 2014)

497

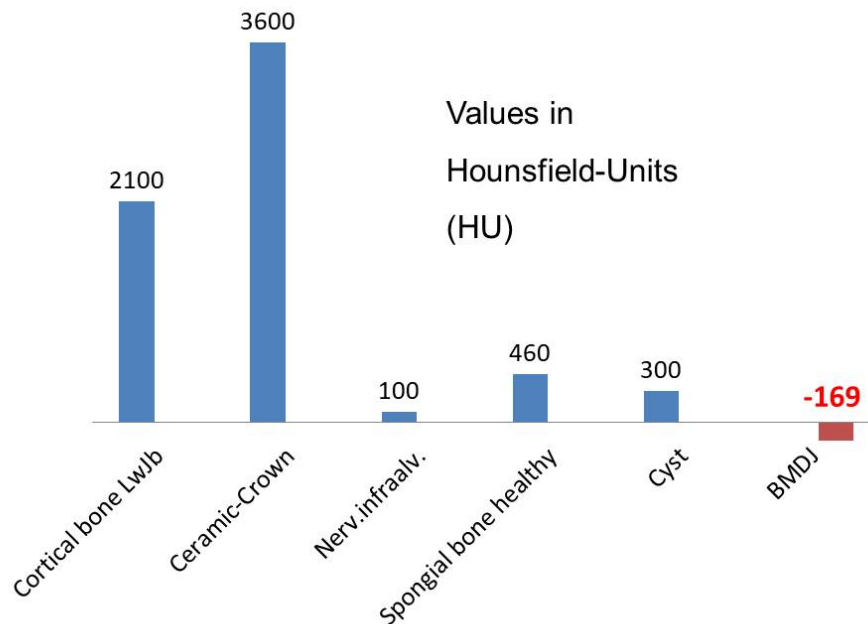
498

499

500 *On "bone marrow defects" and 3D-DVT*

501 As with the 2D-OPG radiographs, in order to compare the results documented  
 502 in Table 1 in terms of their clinical significance, we calculated 10 mean values of 3D-  
 503 DVT measurements from three different dental colleagues with existing radiographs,

504 as above. Figure 12 shows these HU values in blue. The bone density value of -169  
505 HU in the BMDJ/FDOJ areas collected from the cohort of 210 patients is presented in  
506 red.



507  
508 Figure 12: Comparison of a wide variety of density values with BMDJ/FDOJ values  
509 obtained with 3D-DVT. This shows that the HU value of -169 produced by the  
510 reduced X-ray attenuation in the softened BMDJ/FDOJ areas is significantly less than  
511 the minimum value of 300 reported as healthy in the literature.

512 A reliable assessment of the medullary bone density in areas of BMDJ/FDOJ is  
513 possible with the HU values derived using high-quality 3D-DVT (Loubele M et al.  
514 2008. Roberts JA, Drage NA, Davies J, Thomas DW. 2009). However, this method of  
515 examination requires a relatively high radiation exposure. Furthermore, DVT devices  
516 which provide the HU measurement necessary are costly. In our experience,  
517 inexpensive DVT units fail to achieve the requisite quality and lead to incorrect  
518 assessments based on purely subjective evaluation.

519

520

521

522 *On "bone marrow defects" and TAU-n*

523         When the TAU-n AverageLog values are compared with the DVT-HU values  
524 determined in this study, both correspond to reduced bone density, which infers the  
525 presence of BMDJ/FDOJ. Further, the general correlation of HU and R/C multiplex  
526 analysis with the "AverageLog" values generated using the TAU-n software may be  
527 confirmed. In previous publications, light microscopy also confirmed the reduction of  
528 bone density determined by the CaviTAU® AverageLog values (Lechner J,  
529 Zimmermann B, Schmidt M, von Baehr V. 2020)

530

531 *The threshold for which TAU-n Log indicates BMDJ/FDOJ*

532         As shown in Table 1, the mean value of 210 TAU-n measurements in  
533 BMDJ/FDOJ areas is 1.2 with a range of 0.3 (#5) to 1.95 (#153). Accordingly, we  
534 defined the threshold for which a TAU-n Log indicates diminished bone density that  
535 corresponds to a BMDJ/FDOJ area at a TAU-n scale of 2. A TAU-n value of 2.29 with  
536 respect to patient #53 was the only measurement determined beyond the threshold  
537 of 2, however, a four-fold overexpression of R/C was also detected in this case.

538

539

540 *RANTES/CCL5 expression in BMDJ/FDOJ*

541         The values of R/C expression in the samples of BMDJ/FDOJ analyzed  
542 postoperatively with multiplex methods in the laboratory average at 1,950.38 pg/ml,  
543 which is 13 times the normal value of 149.9 pg/ml found in healthy jawbone  
544 previously published by the authors (Lechner J, von Baehr 2013). First and foremost,  
545 the application of TAU-n allows for the use of low radiation levels in the stress-free  
546 detection of mineralization and metabolic disorders in the medullary region of the

547 jawbone. Medical devices that aim to measure specific phenomena must be able to  
548 consistently reproduce their results. In this respect, the measurements obtained with  
549 TAU-n are reliable and primarily free of operator errors, as the TAU-n transmitter and  
550 receiver are positioned along a coplanar axis in a fixed arrangement. This ensures  
551 the necessary independence from the operator and the reproducibility of TAU-n  
552 measurements. Errors in acoustic coupling are avoided by displaying a gray sensor  
553 field, which is not associated with ultrasound transmission during the measurement  
554 process.

555

#### 556 *Limits in the comparability of the measured HU and TAU-n values*

557 A 1:1 correlation of the measured values obtained with DVT in HU and using TAU-n  
558 is not possible since both examination methods are physically different and thus  
559 measure different distances in the jaw. However, a general technical correlation may  
560 be made as follows: The measured HU values correspond to a selected cross-  
561 sectional slice of the jaw, while TAU-n penetrates through the entire distance from  
562 the transmitter to the sensor and thus reproduces the typical reflective and scattering  
563 properties of ultrasound. As such, TAU-n is unable to isolate particular sections  
564 within the jawbone. Furthermore, the attenuation coefficients of both methods behave  
565 in completely opposite ways. With HU, the denser the irradiated object, the greater  
566 the positive attenuation coefficients and the lower the transmission. With TAU-n, the  
567 greater the density of the object to be examined, the lower the attenuation  
568 coefficients and, thus, the greater the sound transmission. A relationship between the  
569 two methods may still be established, however, as conspicuous areas assessed  
570 using HU are also detectable with TAU-n and vice versa. To ensure that TAU-n is a  
571 reliable indicator of poor bone quality, this approach should be validated in patients  
572 without BMDJ/FDOJ. Here, we face an ethical obstacle, as patients with HU values

573 >300 and TAU-n Log >2 are inappropriate candidates for jawbone surgery. Thus, it  
574 is not possible to obtain R/C values in such cases. As such, the study design  
575 employed is unable to fully answer the initial question posed in this study.

576

577

## 578 **Summary**

579 The interest in the application of TAU-n lies in the decrease in bone density in  
580 BMDJ/FDOJ due to osteolysis. The upper limit of DVT HU values of interest with  
581 respect to BMDJ/FDOJ is +300, as at this point there is a transition to healthy  
582 cancellous bone. Values over +300 HU thus fall outside the necessary detection  
583 range of TAU-n. The HU values produced in this study (range: -680 to +150) indicate  
584 BMDJ/FDOJ in class 5 cases (Mah et al., 2010). The data presented here shows  
585 that HU values demonstrate osteolysis and these values also correspond to R/C  
586 overexpression in BMDJ/FDOJ areas (Lechner et al., 2018). When the data derived  
587 from both methods used to evaluate BMDJ/FDOJ (i.e., HU values and R/C  
588 expression) are compared with the TAU-n results, there is a correlation between the  
589 attenuation coefficients of HU and TAU-n. Thus, it may be assumed that TAU-n,  
590 which uses ultrasound waves, is able to provide an accurate representation of the  
591 degrees of mineralization and bone density in the jawbone area.

592

- 593 ▪ Using the AverageLog values generated with TAU-n, we confirmed a general  
594 correspondence between HU values and R/C multiplex analysis in a cohort of  
595 210 BMDJ/FDOJ patients.
- 596 ▪ Table 1 shows two cases (#53 = 2.29 and #123 = 2.67) with an AverageLog  
597 value of >2 from the total of 210 cases.

598     ▪ Here, HU values and postoperatively measured levels of cytokine expression  
599         confirm the reliability of TAU-n measurements with respect to displaying  
600         decreased bone density in cases of BMDJ/FDOJ.

601

## 602     **Conclusion**

603             A newly developed ultrasonography device (TAU-n) is able to detect and  
604     localize BMDJ/FDOJ caused by the fatty degenerative dissolution of medullary  
605     trabecular structures in the jawbone. As other studies have confirmed (Guglielmi  
606     and de Terlizzi, 2009; Komar et al., 2019), ultrasonography is a low cost and  
607     efficient means of assessing jawbone health, and this was replicated with the use of  
608     the new TAU device presented here. This study established a new value using  
609     TAU-n which provides a reliable indicator of poor bone quality, rendering the device  
610     a useful tool for treatment planning strategies in implantology, as well as for  
611     fostering cooperation among professionals when assessing or treating  
612     osteimmunological diseases and linking such diseases with the immune system.  
613     TAU-n thus provides a non-harmful alternative to the use of X-ray irradiation, which  
614     is increasingly criticized (Brenner et al., 2001; Vano et al., 2017), particularly in view  
615     of more stringent radiation protection laws (Strahlenschutzgesetz, 1966). TAU-n  
616     represents a novel type of imaging acquisition process in dentistry and offers the  
617     ability to non-invasively assess hidden BMDJ/FDOJ in the human jawbone. Further  
618     extensive clinical trials and multicenter comparative measurements examining TAU-  
619     n should be carried out to establish a new classification based on ultrasound and  
620     perform a reliability assessment.

621

## 622     **Limitations**



623           The limitations of this study include the sample size employed. Bias may also  
624 be present due to the fact that not all parameters were validated in the healthy  
625 jawbone patient cohort. For ethical reasons, surgical intervention and the  
626 measurement of R/C expression in healthy jawbone, without any sign of  
627 BMDJ/FDOJ, was not applicable.

628

### 629 **Conflicts of Interest**

630 CaviTAU® (Munich, Germany), the company that designed the new TAU-n  
631 apparatus and associated software, provided these tools without charge for the  
632 purposes of this study. The ultrasonography procedure was carried out at the Clinic  
633 for Integrative Dentistry (Munich, Germany). CaviTAU® and the Clinic for Integrative  
634 Dentistry are engaged in ongoing discussions regarding numerous collaborative  
635 arrangements to further improve and verify the new TAU apparatus, CaviTAU®, as it  
636 is introduced to the market. The corresponding author is the holder of a patent used  
637 in CaviTAU®.

638

### 639 **Acknowledgments**

640 English-language editing of this manuscript was provided by Journal Prep Services.  
641 Additional editing was provided by Natasha Gabriel. The practical measurements  
642 with TAU-n were performed at our clinic by Gabriele Zidek and Tanja Scheller.

643

644 **References**

645

646

647 Al-Nawas B, Grotz KA, Kann P. Ultrasound transmission velocity of the irradiated jaw  
648 bone in vivo. Clin Oral Investig 2001;5(4):266-8.

649 Bouquot JE, Roberts AM, Person P, Christian J. Neuralgia-inducing cavitational  
650 osteonecrosis (NICO). Osteomyelitis in 224 jawbone samples from patients  
651 with facial neuralgia. Oral Surg Oral Med Oral Pathol 1992;73(3):307-19.

652 Brenner D, Elliston C, Hall E, Berdon W. Estimated risks of radiation-induced fatal  
653 cancer from pediatric CT. AJR Am J Roentgenol 2001;176(2):289-96.

654 Greenfield MA, Craven JD, Huddleston A, Kehrer ML, Wishko D, Stern R.  
655 Measurement of the velocity of ultrasound in human cortical bone in vivo.  
656 Estimation of its potential value in the diagnosis of osteoporosis and metabolic  
657 bone disease. Radiology 1981;138:701-10.

658 Guglielmi G, de Terlizzi F. Quantitative ultrasound in the assessment of osteoporosis.  
659 Eur J Radiol 2009;71(3):425-31.

660 Kaufman JJ, Einhorn TA. Ultrasound assessment of bone. J Bone Miner Res  
661 1993;8:517-25.

662 Klein MO, Grotz KA, Manefeld B, Kann PH, Al-Nawas B. Ultrasound transmission  
663 velocity for noninvasive evaluation of jaw bone quality in vivo before dental  
664 implantation. Ultrasound Med Biol 2008;34(12):1966-71.

665 Komar C, Ahmed M, Chen A, Richwine H, Zia N, Nazar A, Bauer L. Advancing  
666 methods of assessing bone quality to expand screening for osteoporosis. J  
667 Am Osteopath Assoc 2019;119(3):147-54.

668 Kumar VV, Sagheb K, Klein MO, Al-Nawas B, Kann PH, Kammerer PW. Relation  
669 between bone quality values from ultrasound transmission velocity and

670 implant stability parameters – an ex vivo study. Clin Oral Implants Res  
671 2012;23(8):975-80.

672 Lechner J, Huesker K, Von Baehr V. Impact of Rantes from jawbone on Chronic  
673 Fatigue Syndrome. J Biol Regul Homeost Agents 2017a; 31:321.

674 Lechner J, Mayer W. Immune messengers in neuralgia inducing cavitation  
675 osteonecrosis (NICO) in jaw bone and systemic interference. Eur J Integr Med  
676 2010;2(2):71-7.

677 Lechner J, Rudi T, von Baehr V. Osteoimmunology of tumor necrosis factor-alpha,  
678 IL-6, and RANTES/CCL5: a review of known and poorly understood  
679 inflammatory patterns in osteonecrosis. Clin Cosmet Investig Dent  
680 2018;10:251-62.

681 Lechner J, Schuett S, von Baehr V. Aseptic-avascular osteonecrosis: local “silent  
682 inflammation” in the jawbone and RANTES/CCL5 overexpression. Clin  
683 Cosmet Investig Dent 2017b;9 99-109.

684 Lechner J, von Baehr V. Chemokine RANTES/CCL5 as an unknown link between  
685 wound healing in the jawbone and systemic disease: is prediction and tailored  
686 treatments in the horizon? EPMA J 2015;6(1):10.

687 Lechner J, von Baehr V. RANTES and fibroblast growth factor 2 in jawbone  
688 cavitations: triggers for systemic disease? Int J Gen Med 2013;6:277-90.

689 Lechner J, Zimmermann B, Schmidt M, von Baehr V. Ultrasound Sonography to  
690 Detect Focal Osteoporotic Jawbone Marrow Defects: Clinical Comparative  
691 Study with Corresponding Hounsfield Units and RANTES/CCL5 Expression.  
692 Clin Cosmet Investig Dent. 2020;12:205-216.  
693 <https://doi.org/10.2147/CCIDE.S247345>

694 Lechner J. Validation of dental X-ray by cytokine RANTES - comparison of X-ray  
695 findings with cytokine overexpression in jawbone. *Clin Cosmet Investig Dent*  
696 2014;6:71-9.

697 Lee SC, Jeong CH, Im HY, Kim SY, Ryu JY, Yeom HY, Kim HM. Displacement of  
698 dental implants into the focal osteoporotic bone marrow defect: a report of  
699 three cases. *J Korean Assoc Oral Maxillofac Surg* 2013;39(2):94-9.

700 Lipani CS, Natiella JR, Greene GW Jr. The hematopoietic defect of the jaws: a report  
701 of sixteen cases. *J Oral Pathol* 1982;11(6):411-6.

702 Loubele M, Bogaerts R, van Dijck E, Pauwels R, Vanheusden S, Suetens P, Marchal  
703 G, Sanderink G, Jacobs R. Comparison between effective radiation dose of CBCT  
704 and MSCT scanners for dentomaxillofacial applications. *Eur J Radiol* 16 July 2008.

705 Mah P, Reeves TE, McDavid WD. Deriving Hounsfield units using grey levels in cone  
706 beam computed tomography. *Dentomaxillofac Radiol* 2010;39(6):323-35.

707 Mahmoud A, Cortes D, Abaza A, Ammar H, Hazey M, Ngan P, Crout R, Mukdadi O.  
708 Noninvasive assessment of human jawbone using ultrasonic guided waves.  
709 *IEEE Trans Ultrason Ferroelectr Freq Control* 2008;55(6):1316-27.

710 Misch CE. Bone density: A key determinant for clinical success. In: Misch CE, ed.  
711 *Contemporary Implant Dentistry*, 2nd ed. St Louis: CV Mosby Company; 1999:  
712 109-18.

713 Njeh C, Hans D, Fuerst C, Gluer C, Genant HK, eds. *Quantitative ultrasound: assessment of osteoporosis and bone status*. United Kingdom: Martin Dunitz, Ltd., 1999.

716 Norton MR, Gamble C. Bone classification: an objective scale of bone density using  
717 the computerized tomography scan. *Clin Oral Implants Res* 2001;12(1):79-84.

718 Roberts JA, Drage NA, Davies J, Thomas DW. Effective dose  
719 from cone beam CT examinations in dentistry. *Br J Radiol* 2009;82:35-40.

720 Strahlenschutzgesetz (StrlSchG) Artikel 1 G. v. 27.06.2017 BGBl. I S. 1966;  
721 Strahlenschutzverordnung (StrlSchV) Artikel 1 V. v. 29.11.2018 BGBl. I S.  
722 2034, 2036; Gesetz zur Neuordnung des Rechts zum Schutz vor der  
723 schädlichen Wirkung ionisierender Strahlung (StrlSchGEG) G. v. 27.06.2017  
724 BGBl. I S. 1966.

725 Swennen GR, Schutyser F. Three-dimensional cephalometry: spiral multi-slice vs  
726 cone-beam computed tomography. Am J Orthod Dentofacial Orthop  
727 2006;130(3):410-6.

728 Vaño E, Miller DL, Martin CJ, Rehani MM, Kang K, Rosenstein M, Ortiz-Lopez P,  
729 Mattsson S, Padovani R, Rogers A; Authors on behalf of ICRP. ICRP  
730 Publication 135: Diagnostic reference levels in medical imaging. Ann ICRP  
731 2017;46(1):1-144.

732 Wells PNT: Ultrasonic imaging of the human body. Rep Prog Phys 1999;62(5):676.  
733

734

735